Picosecond measurements of phenol excited-state proton transfer in clusters. I. Solvent basicity and cluster size effects

J. A. Syage and J. Steadman[a)]
Aerophysics Laboratory, The Aerospace Corporation, Los Angeles, California 90009

(Received 28 March 1991; accepted 9 May 1991)

Excited-state proton transfer (ESPT) rates in molecular clusters were measured as a function of cluster size using picosecond spectroscopy in a molecular beam mass spectrometer. ESPT from the S_1 state of phenol to base solvent clusters $(NH_3)_n$ occurs for a critical solvent cluster size $n \geqslant 5$, with a rate constant of $k = (60 \pm 10\ \text{ps})^{-1}$ for $n = 5$–7. ESPT showing critical cluster-size dependencies was also observed in the basic solvent $N(CH_3)_3$ ($n \simeq 3$). Proton transfer was not observed in the less-basic solvent clusters $(CH_3OH)_n$ and $(H_2O)_n$. Mixed-solvent studies indicate that the addition of a dissimilar molecule to an otherwise neat solvent cluster impedes ESPT, presumably due to a disruption of the hydrogen bonding network. Evidence is also presented for the direct measure of solvent reorganization following ESPT. For $(NH_3)_n$ solvation, the solvent reorganization appears as a long-time-scale component (0.3 ns) on the protonated solvent formation traces.

I. INTRODUCTION

The majority of useful chemistry takes place in solution and is strongly influenced by the properties of the solvent. The dependence of chemical behavior on macroscopic bulk-phase properties (e.g., solvent polarity, viscosity, thermodynamics) is well understood and for the most part described successfully by empirical models and continuum theories.[1–4] Much less is known about the detailed microscopic processes governed by pairwise molecular interactions and local dynamics.[4,5] Molecular clusters represent an ideal medium for studying solute–solvent interactions on a molecular level and for understanding the convergence to condensed-phase behavior by the addition of single solvent molecules.[6–17]

Acid-base proton transfer reactions are quite prevalent in solution,[18–22] yet they are exceedingly rare in the gas phase.[23,24] The reason for this disparity is that the dissociation energy of a proton in a neutral gas-phase molecule is typically ~ 15 eV (about 400 kcal/mol), which we compare to a typical hydrogen atom dissociation energy of 4 eV. The energy difference is due largely to the 13.6 eV ionization potential of the H atom. The fact that proton dissociation occurs under common solution-phase conditions illustrates the enormous stabilization exerted by the solvent. The study of solvation in clusters is a sensitive probe of how reactive potential surfaces are shifted in energy by individual solvent–molecule interactions. It is not often appreciated that acid-base chemistry is electronic in origin. Hence, these reactions are typically governed by potential curve crossings, energy barriers, and geometry constraints. Each of these conditions are dependent on the properties of the solvent. We present results that show how the shape and energies of the reactive potential-energy surface are changed by the addition of single solvent molecules.

Real-time spectroscopy in molecular beams, pioneered by Zewail and co-workers over the last decade,[25–28] has provided a means for studying chemical reactions over very narrow energy distributions and in the absence of interfering effects such as solvent interactions. This work is vital because to understand solvent effects, one must first understand the intrinsic properties of the isolated molecule. A complementary literature has evolved around the study of van der Waals (vdW) dimers in order to understand how the isolated molecule is perturbed by other atoms and molecules.[28–31] These studies are too numerous to summarize; however, some of the time-resolved work revealed pronounced state-specific rates of dissociation.[28–30] These demonstrations of quantum effects at the most elementary level of solvation (i.e., vdW dimer) may presage similar behavior in larger clusters. The use of real-time molecular beam mass spectroscopy for studying reactive molecules in solvent clusters has been reported recently by Ray and Lineberger *et al.* for I_2^- dissociation and recombination in $(CO_2)_n$ clusters,[16] by Breen and Zewail *et al.* for excited-state 1-naphthol proton transfer in $(NH_3)_n$ clusters,[17] and by Steadman and Syage for free radical chemistry in $(CH_3I)_n$ clusters[12] and excited-state proton transfer of phenol in $(NH_3)_n$ clusters.[13–15] In related time-resolved work, Brucker and Kelley have measured proton transfer rates for aromatic hydroxy molecules in small solvent complexes formed on cryogenic surfaces.[32]

In an earlier communication, we reported picosecond measurements of reactant cluster decay and product formation for excited state (S_1) phenol proton transfer in $(NH_3)_n$ clusters.[13] This work expands on those results by presenting the dependence of the phenol reaction on other solvent and mixed solvent clusters, allowing us now the independent parameters of cluster size and solvent proton affinity (basicity). The results show that stabilization by individual solvent molecules is not simply additive, but that there are cooperative effects that depend on the ability of the solvent cluster to form an optimum hydrogen bonding network. The focus of the discussion is on the energetics and structure of the microsolvent clusters. We present a model for stepwise solvation from which potential energy curves were obtained as a function of cluster size. In a companion paper (referred to as paper II),[14] we report on the reactivity of phenol cation

[a)] National Research Council postdoctoral associate.

 0021-9606/91/162497-14$03.00

in solvent clusters and derive solvent-modified potential energy curves in the context of ion–molecule reactions.

II. EXPERIMENTAL

A pulsed (10 Hz) active/passive mode-locked and amplified Nd:YAG laser was used to produce frequency doubled (532 nm, 25 ps), tripled (355 nm, 25 ps), and quadrupled (266 nm, 18 ps) output and to pump a short-cavity tunable dye laser (10 ps).[12–15] A typical optical setup is illustrated in Fig. 1. The pump λ_1 excitation was usually provided by 266 nm pulses or frequency-doubled dye laser pulses. The probe λ_2 excitation was supplied by either the 532 or 355 nm Nd:YAG harmonics, or by the dye laser fundamental and/or frequency-doubled output. In the latter case, the 532 nm (20 mJ) Nd:YAG output was split into equal portions to pump the dye laser (580–600 nm, 10 ps, 0.5–1.0 mJ) and a doubling crystal (266 nm, 0.4 mJ). The λ_1 and the λ_2 pulses traveled along separate variable-delay lines and were then combined using a dichroic beam splitter and steered collinearly into the molecular beam apparatus. Polarizing attenuators and neutral density filters were used to reduce pulse energies. Typical pulse energy densities for this study were λ_1 (266 nm, 20 μJ, 2 mm diam) and λ_2 (532 nm, 1 mJ, 3 mm diam or 355 nm, 0.5 mJ, 3 mm diam). Time-resolved spectra were recorded by delaying λ_2 relative to λ_1 using a scanning optical delay line. The two-pulse cross-correlation function was measured by sum-frequency generation in a KDP crystal and gave a response that was described well by a Gaussian function. Calculated curves were fitted to time-dependent measurements by convolving with a Gaussian instrument function of width 25 ps for 532 nm probe ionization and 30–35 ps for 355 nm ionization. The 532 nm ionization is typically a two-photon process in the present work, which may account for the narrower correlation time.

The molecular beam time-of-flight (TOF) mass spectrometer is based on differentially pumped source and detection chambers. Details of the vacuum system and data acquisition system have been described before.[11] The source chamber employs a temperature-controlled pulsed nozzle. Typical pulsed expansion conditions were 35 psi He or Ar, 500 μm diam nozzle, 400 μs pulse width, 2 cm nozzle–skimmer distance, and 1 mm diam skimmer. The ambient base pressure in the detection chamber was typically 2×10^{-8} Torr, rising to about 2×10^{-7} Torr during operation of the pulsed nozzle at 10 Hz. Our TOF mass spectrometer is based on the Wiley–McLaren three-grid space focusing design.[33] We use 1 cm grid spacings, a 1 m drift tube, and extraction and acceleration fields of 200 and 1800 V/cm, respectively. Deflection plates are used to compensate for the molecular beam velocity. The deflector voltage is adjusted to optimize the signal for a particular mass range of interest. Mass spectra were recorded by digitizing (100 MHz sampling rate) the amplified current output of a dual microchannel-plate detector. Time-resolved measurements were recorded by integrating specific ion mass signals with a boxcar averager while scanning the picosecond delay line.

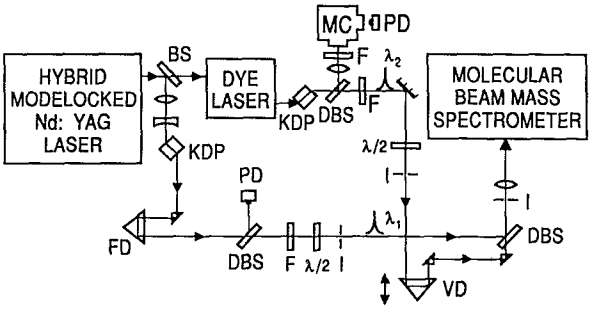

FIG. 1. A typical picosecond pump–probe configuration involving the use of Nd:YAG harmonics and a tunable dye laser. Terms are defined as follows: BS, beam splitter; DBS, dichroic beam splitter; F, filter; FD, fixed delay line; I, iris; $\lambda/2$, half-wave plate; MC, monochromator; PD, photodiode; VD, variable delay line.

Solvated aromatic clusters were prepared by several procedures. In most cases, the aromatic was deposited in a sample holder contained in the pulsed nozzle housing and heated to about 60 °C. For ammonia or trimethylamine solvation, a 2 ℓ high-pressure cylinder was filled with a sample containing 10% gaseous solvent in helium. Water and methanol solvation was achieved by passing the helium flow through a bubbler containing either of these solvents. For the mixed solvent experiments involving NH_3 and a condensable solvent such as H_2O or CH_3OH, the 10% ammonia in helium cylinder sample was passed through the bubbler containing the other solvent.

III. MODEL FOR TIME-RESOLVED SPECTRA

The picosecond pump–probe excitation/detection scheme is given in Fig. 2 and shows approximate potential curves for the relevant ground, excited, and ionic states of the cluster. The potential curves are strongly dependent on solvent cluster size and basicity and are discussed in detail in Sec. V. The illustration given in Fig. 2 approximates the case for phenol-$(NH_3)_5$.

The phenol (PhOH) excited-state proton transfer (ESPT) reaction

$$\mathrm{PhOH^*\cdot B_n} \underset{k}{\rightarrow} \mathrm{PhO^{*-}H^+B_n}$$

corresponds to a conversion from the locally excited S_1 state of the acid phenol to an excited ion-pair state (B_n refers to the base solvent cluster consisting of n molecules). Reactant and product are distinguishable by mass spectrometry because each species fragments differently upon ionization. The energetics and dynamics of the solvent-clustered phenol cation are reported in paper II.[14] Briefly, a double-well minima with a large barrier exists for the cluster ions. As illustrated in Fig. 2, ionization of the reactant cluster $\mathrm{PhOH^*\cdot B_n}$ to the inner ion potential well produces strongly bound $\mathrm{PhOH^+\cdot B_n}$ ions (R^+). The product ion-pair $\mathrm{PhO^{*-}H^+B_n}$ is ionized to the outer ion well, which is weakly bound and therefore readily dissociates to form $\mathrm{H^+B_n}$ ions (P^+).

The time-resolved spectra depend not only on the fraction of reactant and product ion dissociation f_a and f_b, respectively, but also on the ionization efficiencies i_a and i_b from the neutral reactant cluster $\mathrm{PhOH^*\cdot B_n}$ and the product ion-pair cluster $\mathrm{PhO^{*-}H^+B_n}$.[34] These quantities vary

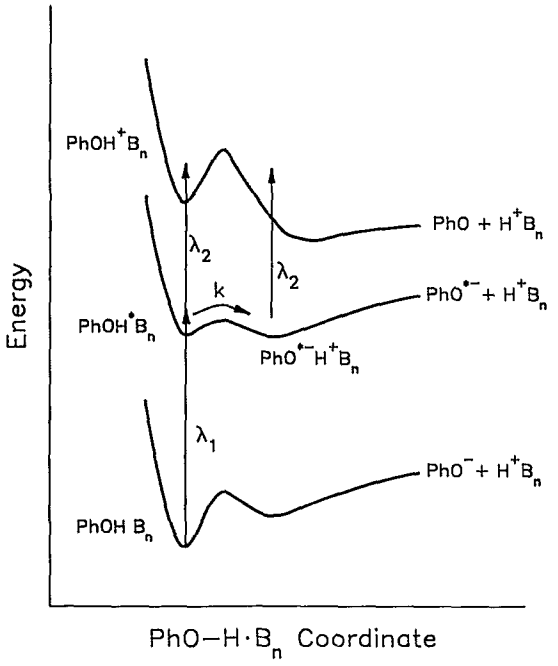

FIG. 2. Energy diagram for PhOH·$(NH_3)_n$ consistent with a cluster size of $n \sim 5$. ESPT produces an excited state ion-pair product that is ionized to the weakly bound outer potential well of the cluster ions.

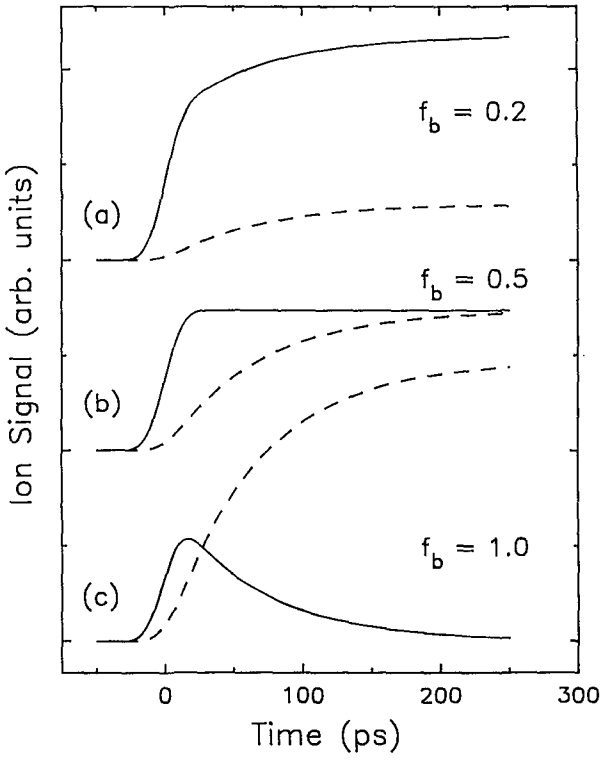

FIG. 3. Calculated reactant $R^+(t)$ [Eq. (1) (—)] and product ion $P^+(t)$ [Eq. (2) (---)] time dependence as a function of outer-well dissociation fraction f_b. Calculations assume $f_a = 0$, $i_b = 2i_a$, and $1/k = 65$ ps. Each plot is on the same relative intensity scale so that signal levels can be compared.

with solvent cluster size and photoionization energy. The time dependence for reactant and product ions R^+ and P^+ is given by

$$R^+(t) = R^*(0)\{i_b(1-f_b) + [i_a(1-f_a) - i_b(1-f_b)]e^{-kt}\}, \quad (1)$$

$$P^+(t) = R^*(0)\{i_b f_b + [i_a f_a - i_b f_b]e^{-kt}\}, \quad (2)$$

where $R^*(0)$ is the initial population of the excited-state reactant PhOH*·B_n. For the ideal case where reactant ionization is undissociative ($f_a = 0$) and product ionization is completely dissociative ($f_b = 1$), the above equations reduce to the simple form

$$R^+(t) = R^*(0)i_a e^{-kt}, \quad (3)$$

$$P^+(t) = R^*(0)i_b(1-e^{-kt}). \quad (4)$$

The 532 nm two-photon ionization from the S_1 state results in nearly ideal behavior for most of the solvents studied (paper II).[14] The 355 nm one-photon ionization leads to incomplete dissociation from the outer well (i.e., $f_b < 1$). The effect of different values of f_b on the time-resolved signals is illustrated in Fig. 3. For $i_b > i_a$, which holds for the solvated phenol clusters,[14] the reactant traces $R^+(t)$ increase in intensity with time for small values of f_b and decay for large values of f_b. Despite this variation of curve shapes, the time dependence for $R^+(t)$ is always due to the ESPT rate constant k. Only when the bracket term preceding the $\exp(-kt)$ term in Eq. (1) is near zero is the time-dependence difficult to measure [cf. Fig. 3(b)]. The shape of the product traces $P^+(t)$ are less sensitive to values of f_a and f_b. Values of $f_a > 0$ add step-function responses to $P^+(t)$; values of $f_b < 1$ change the intensity, but not the shape of the time-varying part of the signal.

IV. RESULTS AND ANALYSIS

The excitation of PhOH·$(NH_3)_n$ to the S_1 electronic state by $\lambda_1 = 266$ nm deposits excess energy ranging from about 1900 cm^{-1} ($n = 1$) to about 2250–2800 cm^{-1} (estimated for $n = 3$–7).[10] The S_1 origin of uncomplexed phenol is at 275.1 nm,[35,36] whereas the cluster onsets are shifted to longer wavelength (280.0, 281.3, and 282.9 nm for $n = 1$–3, respectively; the larger cluster spectra are too diffuse to reliably measure origins).[10,35–38]

The reactive S_1 state was ionized using $\lambda_2 = 355$ or 532 nm excitation. Ionization at 355 nm is by single photon. Ionization at 532 nm leads to greater cluster ion dissociation, suggesting a two-photon process. Although a single 532 nm photon exceeds the measured vertical $E_{I.P.}$ for the larger PhOH·$(NH_3)_n$ clusters [e.g., $E_{I.P.}(n=4) = 6.89$ eV vs $h(\nu_1 + \nu_2) = 6.99$ eV for 266 + 532 nm resonance ionization], the ionization efficiencies at threshold are very small.[10] A mass spectrum is displayed in Fig. 4 showing the series of reactant PhOH$^+$·B_n and product H^+B_n probe signals for B = NH_3 solvation for positive and negative delay time. Pulse energies were reduced to minimize ion intensity due to single-color excitation.

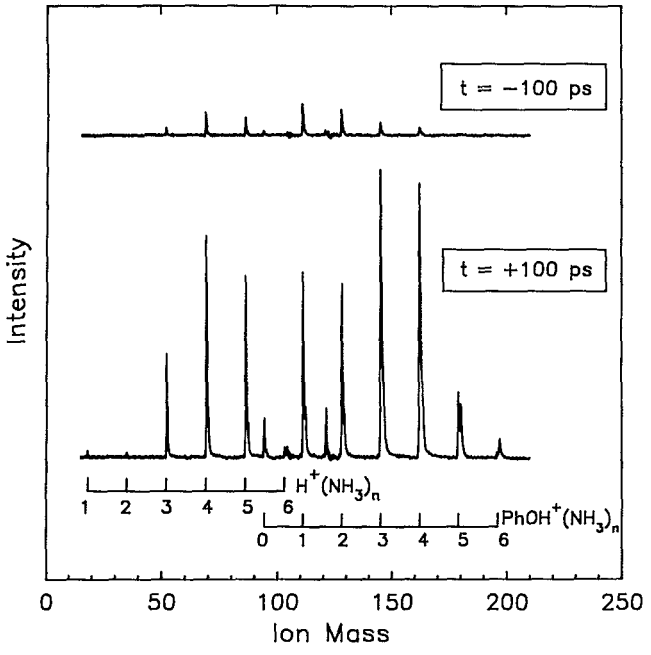

FIG. 4. The two-color picosecond TOF mass spectrum of $PhOH\cdot(NH_3)_n$ for negative and positive relative delay times. Excitation conditions were $\lambda_1 = 266$ nm (~ 20 μJ/pulse, 2 mm diam) and $\lambda_2 = 355$ nm (~ 0.5 mJ/pulse, 3 mm diam). Expansion conditions were 10% NH_3 in He at 35 psi and phenol at 60 °C. The signal at 121 amu is believed to be an impurity. Deflection plates were adjusted to emphasize lower masses.

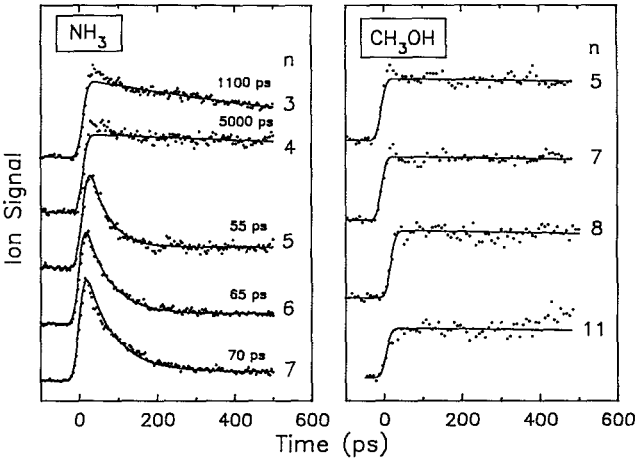

FIG. 5. The observed lifetime of the reactant $PhOH^*\cdot B_n$ (as measured by $PhOH^+\cdot B_n$ detection) in solvent clusters $(NH_3)_n$ and $(CH_3OH)_n$. Excitation conditions were $\lambda_1 = 266$ nm (~ 20 μJ/pulse, 2 mm diam) and $\lambda_2 = 532$ nm (~ 1 mJ/pulse, 3 mm diam). The calculated lifetimes are given next to each curve. The calculated curves through the NH_3 data assume $i_b/i_a = 2.0, f_a = 0$, and $f_b = 0.92$ ($n = 5$), 0.96 ($n = 6$), 0.97 ($n = 7$). Calculated curves assuming a 10 ns lifetime are drawn through the $(CH_3OH)_n$ data.

A. Basicity and solvent-size dependence

A set of reactant decay measurements $R^+(t)$ are presented in Fig. 5 ($\lambda_2 = 532$ nm) as a function of solvent cluster size n for the solvents NH_3 and CH_3OH. The NH_3 solvent clusters induce ESPT for solvent sizes $n > 4$. The solvent $N(CH_3)_3$ was also studied and gave evidence of a reactive threshold at $n \simeq 3$ as discussed in Sec. IV D. No evidence of reaction was observed for CH_3OH (up to $n = 11$, Fig. 5) or H_2O (up to $n = 6$) by time-resolved measurements of reactant. Small residuals of the $n > 4$ decay traces for NH_3 solvation are observed on the $n = 3$ and 4 traces in Fig. 5 due to a minor evaporation of the cluster ions. The reaction rates for $PhOH^*(NH_3)_n$ are plotted in Fig. 6 in the form of a *single-molecule titration curve*. The $(NH_3)_n$ solvent proton affinity (Table I) and calculated enthalpy are discussed in Sec. V.

Product formation kinetics, as measured by the ion-pair dissociative ionization signal $H^+(NH_3)_n$, are given in Fig. 7. This signal, as discussed in paper II, arises predominantly by ion-pair ionization to the weakly bound outer potential well of the cluster ion.[14] Hence, the absence or presence of H^+B_n is a signature for whether or not ESPT occurs for a particular solvent. Formation kinetics are observed for values of n less than the reaction threshold of $n = 5$ because the exothermicity of the cluster ion dissociation causes some evaporation [typically one or two molecules depending on the photoionization energy (Sec. VI C)].[15] The formation curves in Fig. 7 have two time dependencies—a fast one ($\simeq 65$ ps) which matches the decay of reactant in Fig. 5 and a slow one (0.3 ns), which we attribute to solvent reorganization. The model and calculated curves describing these processes are discussed in Sec. VI A.

The reaction rate of $PhOH^*\cdot(NH_3)_n$ is not very sensitive to n above the reaction cluster size threshold ($1/k = 60 \pm 10$ ps for $n = 5$ and ~ 65 ps for $n = 6,7$). One might expect more variation in rate with n, considering that the stabilization energy for each successive solvent molecule is large in these small clusters (Table I). The addition of solvent molecules should reduce the reaction barrier and cause an acceleration of rate. Countering this effect, however, is the increased density of states in larger clusters, which should suppress reaction rates according to RRKM

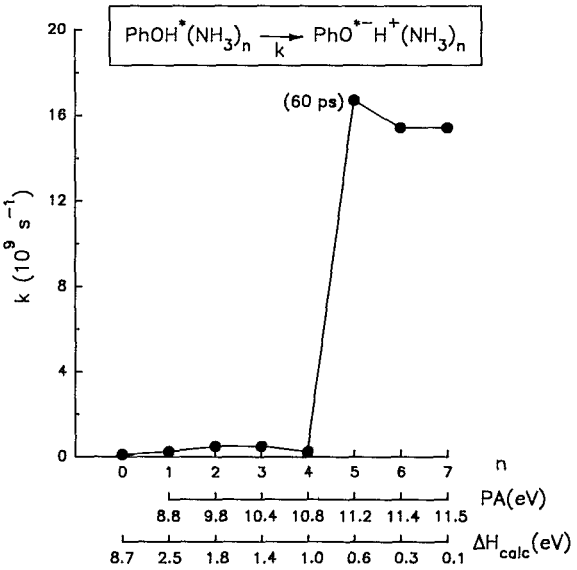

FIG. 6. The single-molecule titration curve relating k to the solvent cluster size n, proton affinity PA, and calculated enthalpy ΔH_{calc}. The rates are averages over many measurements.

TABLE I. Stepwise solvation energies for the reaction $H^+B_{i-1} + B \rightarrow H^+B_i$ and solvent cluster proton affinities (eV) (1 eV/molecule = 23.06 kcal/mol).[a]

	$B = NH_3$			$B = CH_3OH$			$B = H_2O$		
i,n	$D^{H^+}_{i,i-1}$	$\Sigma_i^n D^{H^+}$	$D^{H^+}_n$	$D^{H^+}_{i,i-1}$	$\Sigma_i^n D^{H^+}$	$D^{H^+}_n$	$D^{H^+}_{i,i-1}$	$\Sigma_i^n D^{H^+}$	$D^{H^+}_n$
1	8.84	8.84	8.84	7.90	7.90	7.90	7.36	7.36	7.36
2	1.08	9.92	9.77	1.44	9.34	9.04	1.37	8.73	8.43
3	0.76	10.68	10.38	0.92	10.26	9.66	0.85	9.58	8.98
4	0.60	11.28	10.83	0.70	10.96	10.06	0.78	10.36	9.46
5	0.54	11.82	11.22	0.59	11.55	10.35	0.55	10.91	9.71
6	0.33	12.15	11.40	0.54	12.09	10.59	0.50	11.41	9.91
7				0.52	12.61	10.81	0.46	11.87	10.07
8				0.52	13.13	11.23	0.43	12.30	10.20
∞	0.15[b]			0.30[c]			0.30[d]		

[a] $D^{H^+}_{i,i-1}$ values are from Refs. 6 and 46. The solvent cluster proton affinity is approximated as $D^{H^+}_n = \Sigma_i^n D^{H^+}_{i,i-1} - n \times D_\infty$, where the latter is the neutral–neutral hydrogen bond energy which we equate to $D^{H^+}_{i,i-1}$ in the limit of $i \rightarrow \infty$.

[b] From Refs. 48 and 76.

[c] Reference 77.

[d] We assume the same value as for CH_3OH.

arguments.[39] Further complicating the dynamics is that tunneling may be involved in the barrier crossing.[19] Future work will explore these issues by varying the excitation energy, examining substituent and deuteration effects, and applying more accurate potential curves and quantum statistical analysis (e.g., RRKM) to the measured rates.

Solgadi and co-workers measured the ionization potential ($E_{I.P.}$) of phenol-$(NH_3)_n$ clusters using two-color resonance ionization and observed an abrupt reduction of $E_{I.P.}$ (of 0.62 eV) in going from $n = 3$ to 4.[10] They attribute the result at $n = 4$ to production of the neutral proton-transfer ion-pair state, which has a lower ionization potential than the locally excited S_1 state (cf. Fig. 2). However, our results indicate that the excited state clusters are long lived ($\gg 1$ ns) for $n = 4$ and short lived ($\leqslant 70$ ps) only for $n > 4$. One possibility for the discrepancy between the two experiments is that our $n = 4$ trace is not revealing the reaction because of a low probability of cluster ion dissociation in the outer well [i.e., $f_b < 1$ in Eq. (1)]. For a restricted set of conditions, a null result can occur in the decay curves, as discussed in Sec. III and illustrated in Fig. 3(b). However, the enthalpy of cluster ion dissociation is not sufficiently different between $n = 4$ and $n = 5$ to account for a dramatic difference in f_b values.[14] Alternatively, it is possible that the $E_{I.P.}$ measurements by Solgadi *et al.* are responding to a particularly stable $n = 4$ cluster ion, which could cause a decrease of $E_{I.P.}$ relative to $n = 3$ in the inner potential well. The $n = 4$ cluster should be especially stable since it corresponds to a closed cluster shell about NH_4^+ [i.e., $NH_4^+(NH_3)_3PhO$]. This structure is analogous to the stable (magic number) closed-shell cluster ion $NH_4^+(NH_3)_4$.[40,41]

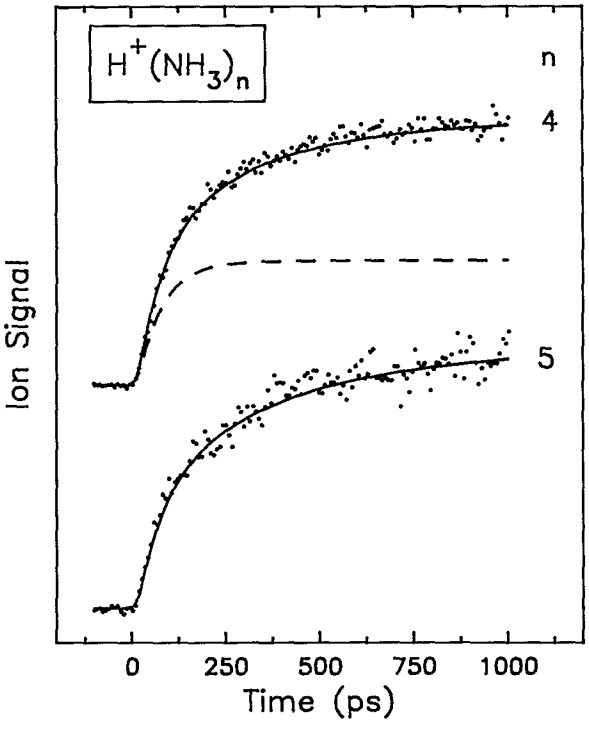

FIG. 7. Observed ESPT $PhO^{*-}H^+B_n$ ion-pair formation kinetics (as measured by H^+B_n detection) for NH_3 solvation. Traces were recorded using 266 nm pump and 532 nm probe excitation. The data were fitted to Eqs. (8) and (9), assuming $1/k = 65$ ps and $f_b = f_c = 1.0$ for $n = 4,5$; and $1/k_s = 350$ ps, $i_c/i_b = 2.4$ (for $n = 4$); and $1/k_s = 300$ ps, $i_c/i_b = 2.0$ (for $n = 5$). The dashed curve assumes $k_s = 0$.

B. Dependence of kinetic traces on ionization energy

The model in Sec. III describes how the shape of the measured kinetic curves depend on the ionization efficiencies and cluster-ion dissociation efficiencies. The ion-pair states of the neutral cluster are strongly bound (~ 3 eV) because of Coulombic attraction (Sec. V). This interaction is lost in the cluster ion, leaving only the weaker charge-dipole and charge-induced dipole interactions ($\leqslant 1$ eV) to bind the protonated solvent cluster to PhO in the outer potential well. The weakly bound outer-well cluster ion dissociates readily, which makes the detection of H^+B_n a convenient probe of ESPT.[14] Nonetheless, it is possible to ionize with sufficiently low energy to avoid extensive dissociation

(i.e., $f_b < 1$). This is the case for 355 nm one-photon ionization of phenol in $(NH_3)_n$ solvent clusters. A set of kinetic traces for $[PhOH]^+ \cdot (NH_3)_n$ and $H^+(NH_3)_n$ using $\lambda_2 = 355$ nm is presented in Fig. 8. The ESPT time dependence for the $[PhOH]^+ \cdot (NH_3)_n$ signal that is so prominent using 532 nm two-photon ionization (Fig. 5) is barely discernible in Fig. 8. The contrasting behavior for the two ionization energies is due to different values of f_b from the outer potential well, as described by the model in Sec. III (and Fig. 3). If we assume $i_b \sim 2i_a$ (which is in good overall agreement with the results in paper II),[14] then the kinetic traces are consistent with values of $f_b \sim 0.5$ for $\lambda_2 = 355$ nm and $f_b \sim 1.0$ for $\lambda_2 = 532$ nm. A slight evidence of decay is seen in Fig. 8 for $n = 6$, which was fit to a function with $f_b = 0.65$.

C. Mixed solvents—disruption of the solvent shell

Mixed solvents were used in an effort to vary basicity for specific cluster sizes. We present measured reactant decay traces in Fig. 9 for different solvent distributions $[PhOH]^*(NH_3)_n(CH_3OH)_m$ of similar cluster size $(n + m = 6$ or 7). Whereas excited phenol in neat NH_3 solvent cluster $(n,m) = (6,0)$ decays in 65 ps, the substitution of a single CH_3OH molecule for NH_3 to give a (5,1) cluster slows the decay to 750 ps. Interestingly, because the (5,0) cluster reacts in 60 ps (Fig. 6), the addition of a CH_3OH molecule reduces the reaction rate by more than an order of magnitude, even though one would expect the proton affinity of the larger solvent size to be greater. One explanation for the slower reaction is that CH_3OH acts as an intruder that disrupts the hydrogen bonding network of the neat $(NH_3)_n$ solvent structure that is crucial to solvating and stabilizing the dissociated proton.[42,43] The following observations regarding the mixed solvent structure may be relevant: (1) the hydroxy proton of phenol bonds to NH_3 rather than CH_3OH[14] and (2) CH_3OH is capable of forming a strong bond to the phenol oxygen, whereas NH_3 avoids that

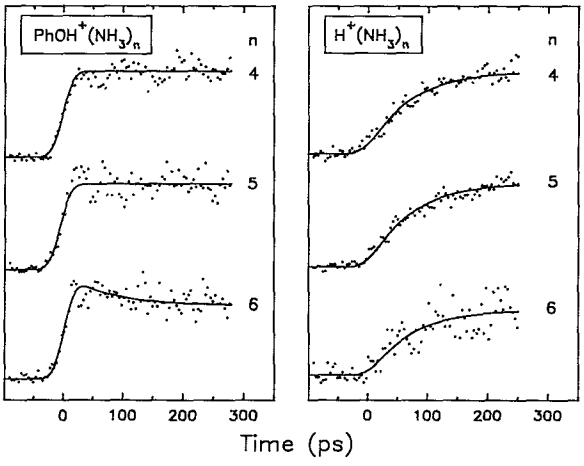

FIG. 8. Reactant (R^+) and product (P^+) time dependencies for NH_3 solvation measured using 266 nm pump and 355 nm probe excitation. The R^+ data were fitted to Eq. (1) for $f_a = 0$, $i_a/i_b = 2.0$, and $f_b = 0.5$ and 0.65 for $n = 4.5$ and $n = 6$, respectively. The P^+ data were fitted to Eq. (4) for convenience, even though a second time constant becomes evident at longer times [cf. Fig. 7, Eq. (8)].

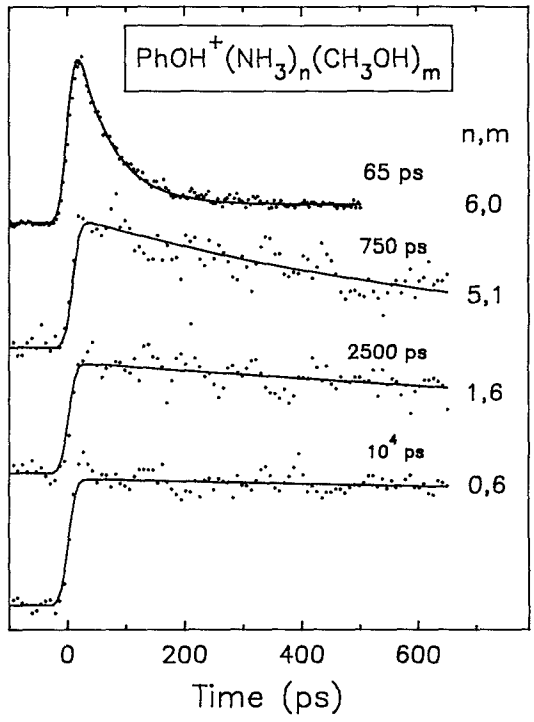

FIG. 9. Measured rates of ESPT for the mixed solvent clusters $PhOH^*(NH_3)_n(CH_3OH)_m$ using 266 nm pump and 532 nm probe excitation. The calculated time constants $1/k$ (ps) were obtained by fitting Eq. (3) to the data.

site.[44,45] It is not known whether CH_3OH acts as a proton acceptor and binds to NH_3, or a proton donor and binds to the phenol oxygen in the mixed solvent cluster.

The concept of critical solvent structures in ESPT reactions has been investigated in the solution phase by Robinson and co-workers.[42] Their picosecond measurements and theoretical analyses on aromatic acids (e.g., 1- and 2-naphthol) in H_2O and alcohol (CH_3OH and C_2H_5OH) mixtures support the notion that a specific solvent structure is necessary to promote proton transfer. They concluded that a critical solvent cluster core was necessary to act as an efficient proton acceptor. For naphthol in solution, the critical solvent-core size for H_2O is about four.[42] Regarding the present results, it is known from gas-phase cluster studies that the closed-shell structure $NH_4^+(NH_3)_4$ is very favorable for stabilizing a proton.[6,41,46] The presence of CH_3OH can disrupt this structure because the NH_3–CH_3OH bond is stronger than the NH_3–NH_3 bond.[47,48] Hence, CH_3OH can "force" its way into the first solvation shell and prevent a pure NH_3 closed-shell structure from forming. The structure of the solvent about a reactive solute molecule has never been measured directly. Studies of cluster distributions for mixed solvent systems are beginning to yield information on the bonding structure of the solvent.[49,50] These investigations should provide new insight into the influence of solvent structure on chemical reactivity.

D. The case for trimethylamine (TMA) solvation

Our studies using $N(CH_3)_3$ (henceforth TMA) cluster solvation gave some bewildering results, although distinct

cluster-size-specific rates were measured that seem attributable to ESPT. We report these results for the sake of completeness. TMA is an interesting cluster solvent because it has a very large proton affinity (9.8 eV),[51] but cannot form a strong hydrogen bonding network. We were curious to know whether this strong gas-phase base might prove to be a poor base in clusters and condensed phase.

Unlike the other solvents studied, the ionization potential of TMA (7.81 eV)[52] is less than that of the chromophore phenol (8.51 eV).[10] Following ionization of $PhOH\cdot(TMA)_n$, an intracluster electron transfer can take place in competition with the dissociative proton transfer that we rely on to probe ESPT. We summarize a few observations from Figs. 10 and 11 that are specific to TMA: (1) the presence of a strong unprotonated TMA^+ signal and the absence of a $PhOH^+$ signal (Fig. 10); (2) the absence of protonated solvent signal $H^+(TMA)_n$ for values $n>2$ (Fig. 10); and (3) the unusual and baffling time dependencies for the $PhOH^+(TMA)_n$ and $H^+(TMA)_n$ signals (Fig. 11), compared to the sensible time-resolved signals for NH_3 solvation in Figs. 5–8. We interpret the presence of $H^+(TMA)_n$ in Fig. 10 as evidence that ESPT occurs and the abrupt change in the $PhOH^+(TMA)_n$ time dependence at $n=3$ in Fig. 11 as an indication of the critical cluster size. A mechanism that describes our results is given by

$$[PhOH]^+\cdot(TMA)_n \rightarrow [PhOH]\cdot(TMA)_n^+$$
$$\rightarrow \begin{cases} PhOH + TMA^+ & (n=1) \\ [PhOH]\cdot(TMA)^+_{n-m} + (TMA)_m & (n>1) \\ PhO + H^+(TMA)^+_{n-m} + (TMA)_m & (n>2) \end{cases}.$$

The model assumes a fast electron transfer followed by one of three possible cluster-size-dependent dissociations. For $n=1$, only one bond can break, thus producing TMA^+. The presence of TMA^+ and absence of $PhOH^+$ in Fig. 10 confirms the electron transfer step.[53] Cluster ions for $n>1$ dissociate preferentially a neutral TMA to preserve the stronger cluster ion–dipole bond(s). Thus, unprotonated $(TMA)_n^+$ is not observed for $n>1$ in Fig. 10. For $n>2$, ESPT is presumed to occur, leading to the formation of neutral excited state ion pairs, which then undergo dissociative ionization to the outer-cluster ion potential well. The ion $H^+(TMA)_{n-m}$ is not observed for $n-m>2$ because TMA forms only a limited hydrogen-bonding network. The closed solvent-shell structure for protonated TMA is $(CH_3)_3N\cdot H^+\cdot N(CH_3)_3$ (cf. Sec. VI C).

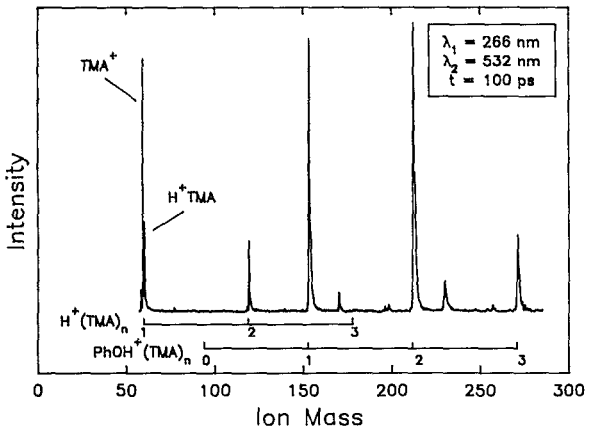

FIG. 10. The two-color picosecond TOF mass spectrum of $PhOH\cdot(TMA)_n$ clusters. Excitation conditions were $\lambda_1 = 266$ nm (10 μJ, 2 mm diam) and $\lambda_2 = 532$ nm (1 mJ, 3 mm diam). An NH_3 impurity gives rise to the weak $[PhOH]^+NH_3(TMA)_n$ signals at 170 and 229 amu.

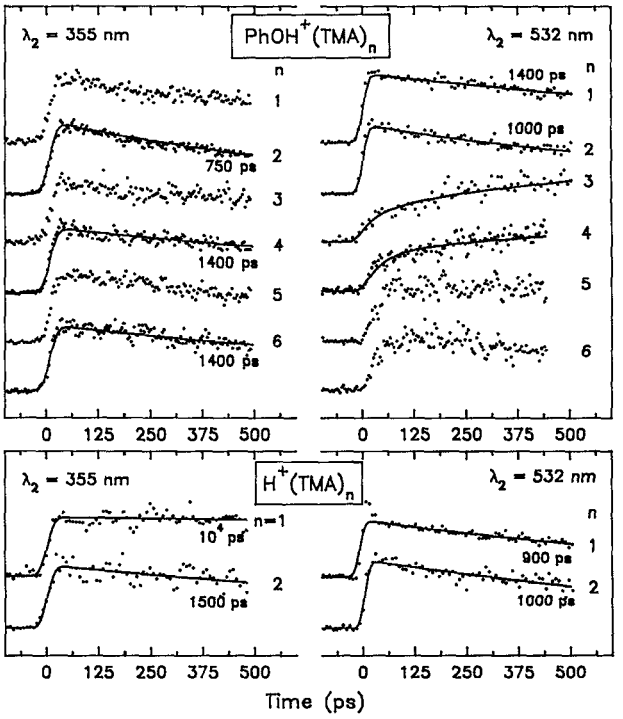

FIG. 11. Reactant (R^+) and product (P^+) time dependencies for TMA solvation measured using 266 nm pump and 355 or 532 nm probe ionization. Single-exponential decay curves [Eq. (3)] are drawn through some of the data for clarity. These are identified by the calculated $1/k$ time constants (ps) listed next to each trace. The $n=3,4$ data for $\lambda_2 = 532$ nm were fitted to the following exponential time constants $(1/k, 1/k_s)$: (50, 800) for $n=3$; and (50, 1000) for $n=4$.

Measurements of $PhOH^*\cdot(TMA)_n$ S_1 lifetime are presented in Fig. 11. The 532 nm ionization results show an abrupt change in behavior at $n=3$. Because of the ion intracluster electron transfer and the lack of a strong hydrogen-bonding solvent network, the measured time-resolved traces may reflect dynamics other than just ESPT. Our discussion of these results are therefore tentative. The $\lambda_2 = 355$ nm data are fitted to Eq. (3) for convenience, although these traces probably reflect more complicated kinetics. The $\lambda_2 = 532$ nm data can be fitted to Eq. (1) if we assume $f_b < (i_b - i_a)/i_b$ for $n=3,4$ and $f_b \simeq (i_b - i_a)/i_b$ for $n=5,6$. One would then assume a slow ESPT reaction ($1/k = 500$–1000 ps). However, this simple explanation overlooks two observations: (1) there appears to be a fast component present in the $[PhOH]^+\cdot(TMA)_n$ traces and (2) the $H^+(TMA)_n$ signal decreases rather than increases with time. An alternative explanation is that a fast ESPT occurs to an unrelaxed solvent structure, followed by a slower solvent reorganization. The Franck–Condon factors to ionization would improve as the unrelaxed structure rear-

ranged about the newly formed proton. The $[PhOH]^+ \cdot (TMA)_n$ traces in Fig. 11 ($n = 3,4$; $\lambda_2 = 532$ nm) were fitted to a double-exponential function and yielded time constants of 50 and 800 ps ($n = 3$) and 50 and 1000 ps ($n = 4$). The decaying $H^+(TMA)_n$ signal is explained by Franck–Condon factors that become more diagonal by solvent relaxation and, therefore, produce lower-energy cluster ions that undergo less dissociation.

The ESPT kinetics are not evident using $\lambda_2 = 355$ nm, possibly because of a near-null condition, as discussed in Sec. III, involving the parameters i_a, i_b, and f_b in Eq. (1). Neither 355 nor 532 nm ionization leads to extensive cluster ion dissociation following ESPT, as indicated by the lack of a strongly decaying $[PhOH]^+ \cdot (TMA)_n$ signal. By this measure, 532 nm ionization appears less dissociative than 355 nm ionization, opposite to that observed for $(NH_3)_n$ solvation. These results suggest that 532 nm ionization is an efficient one-photon process in TMA vs two photon in NH_3. This crossover point is accountable by the increased proton affinity of TMA (9.76 vs 8.84 eV for NH_3),[51] which lowers the energy of the outer-cluster ion potential well proportionately (Fig. 2).

V. POTENTIAL ENERGY CURVES FOR SEQUENTIAL SOLVATION

The addition of single solvent molecules can have large effects on the electronic properties of small clusters. Witness the dramatic changes in chemical behavior at critical cluster sizes in Fig. 5. These incremental effects diminish as the cluster size increases and approaches the bulk-phase limit. For the small clusters studied here, the incremental changes are significant. In this section we construct potential energy curves for the relevant electronic states that are involved in the ESPT reaction. The curves in Fig. 12 are drawn by assuming Morse potentials for covalent bonds and Coulombic potentials for ion-pair bonds.

A. Covalent bonding states

The potential curves of the isolated phenol molecule are given in Fig. 12(a). The energies of the $S_0 \rightarrow S_1$ origin transition and the $E_{I.P.}$ are 4.51 and 8.51 eV, respectively.[35,36] The PhO–H bond energy is $D = 3.75$ eV[54] in S_0 and estimated to be about 3.8 eV[14] in the ground state cation (we assume 3.8 eV for S_1 as well). The potential curves are fit to a Morse function of the form

$$V(r) = D\{1 - \exp[-\beta(r - r_e)]\}^2. \tag{5}$$

We assume an equilibrium O–H bond length of $r_e = 0.95$ Å.[49] The vibrational amplitude is calculated from the classical turning points of a harmonic oscillator. For an O–H $v = 1$ fundamental of frequency 3500 cm^{-1}, one obtains $|r_{max} - r_e| = 0.16$ Å.[55] The excited-state ionic curve that correlates to the dissociative limit $PhO + H^+$ is discussed in paper II.[14]

The addition of a single NH_3 molecule does not change the shape of the PhO–H potential curves for the S_0, S_1, and ionic ground states nearly as much as it lowers the energies relative to uncomplexed phenol [Fig. 12(b)]. These shifts, obtained from measured transition frequencies and ionization potentials, are -0.29, -0.36, and -0.87 eV for S_0, S_1, and the ground state cation, respectively.[10,35] The minima positions as a function of n are tabulated in Table II. The potential curves for $n = 5$ are shown in Fig. 12(c).

B. Ion-pair bonding states

The ion-pair states formed by ESPT correspond to charge transfer (CT) states in the isolated PhOH molecule. The potential energy curve for CT states can be calculated from the sum of the pairwise Coulombic attraction and repulsion interactions. The pairwise potential interaction between specific sites i and j (e.g., atoms within a molecule or cluster) can be expressed as

$$V_{ij} = \frac{q_i q_j}{r_{ij}} + A \exp\left(-\frac{r_{ij}}{\rho}\right), \tag{6}$$

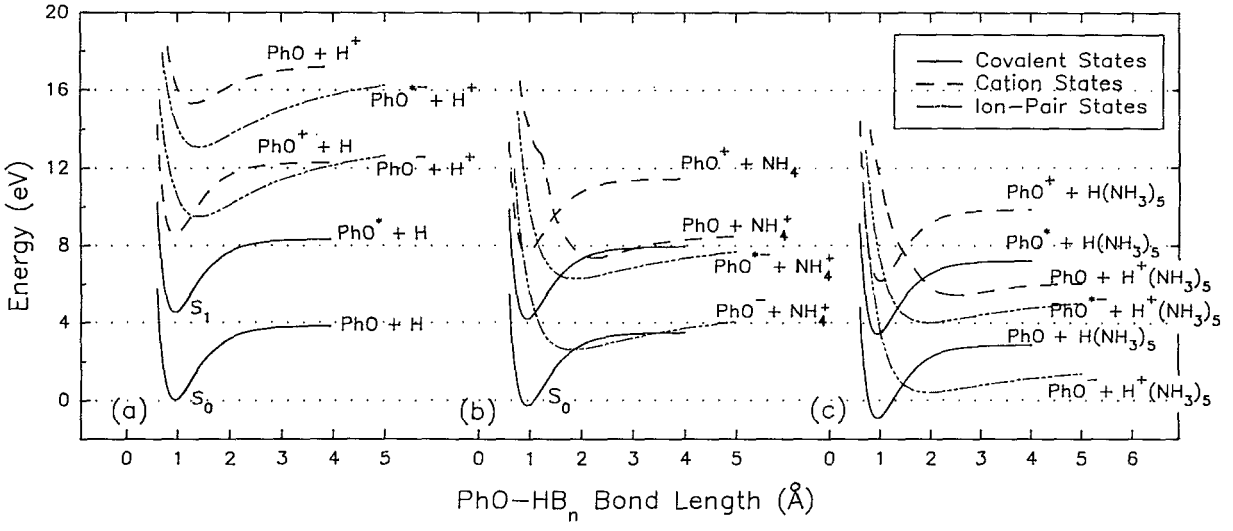

FIG. 12. Approximate $PhOH \cdot (NH_3)_n$ cluster potential energy curves for the reactive PhO–H coordinate. (a) $n = 0$; (b) $n = 1$; and (c) $n = 5$.

TABLE II. Energies of some solvated phenol electronic states (eV) relative to PhOH + $n(NH_3)$ (1 eV/molecule = 23.06 kcal/mol).[a]

n	I $PhOH\cdot(NH_3)_n$	II $PhOH^*\cdot(NH_3)_n$	III $PhO^*\cdot H^+(NH_3)_n$	IV $PhO^* + H^+(NH_3)_n$
0	0	4.51	13.3[c]	18.55
1	−0.29[a]	4.15[a]	6.6	9.71
2	−0.49[b]	3.90[b]	5.7	8.63
3	−0.64	3.70	5.1	7.87
4	−0.79	3.55	4.5 ($\geqslant$3.55)[d]	7.27
5	−0.94	3.40	4.0 ($\leqslant$3.40)[d]	6.73
10[e]	−1.64	2.87	3.0	5.34

[a] The $PhOH\cdot NH_3$ bond energies for S_0 and S_1 are reported to be 0.29 and 0.36 eV; respectively (Ref. 35).
[b] Sequential binding energies chosen to converge to the neutral NH_3–NH_3 energy of 0.15 eV (Ref. 76).
[c] Based on calculated $V^*_{e,n}$ (see the text) and asymptotic energies in column IV.
[d] Determined from observed ESPT cluster size threshold at $n = 5$ and known S_1 energies in column III.
[e] We assume that $n = 10$ closely approximates the bulk limit.

where the q's are charge densities separated by distance r_{ij}, and A and ρ are constants.[56] The total potential $V(r)$ for a specific coordinate r is obtained by summing over all i,j combinations. Charge distributions for the PhO^- ground state were obtained from molecular orbital calculations by Taft and co-workers.[57] Charge densities for $H^+(NH_3)_n$ (up to $n = 4$) were calculated by Deakyne.[40] To simplify the analysis, we have grouped charges as explained in the caption to Fig. 13. The Coulombic potential energy $V(r)$ was calculated as a function of the r_{OH} bond length. The location of the minima depends strongly on the repulsive term in Eq. (6). The O–H equilibrium bond length for the $PhOH\cdot NH_3$ ion-pair state has been calculated to be 1.8 Å.[58] The parameters A and ρ in Eq. (6) were determined by choosing reasonable starting values[5] and adjusting them so that a potential minimum occurred at $r_e = 1.8$ Å for $n = 1$. These repulsive parameters ($\beta = 100$ Å^{-1} and $\rho = 0.32$ Å) were used in calculating the potential curves for all values of n in Fig. 13.[59] The calculated ion-pair potentials neglect some potentially important contributions, such as (1) interatomic potential terms (although these should be small relative to V); (2) stabilization of the PhO^- anion by the solvent; and (3) charge redistribution or ion-induced dipole effects that might be transmitted through the O–H bond (i.e., polarizability). The latter effect is analogous to dielectric screening by polar molecules in solution and would reduce the ion-pair dipole strength and Coulombic attraction.[60]

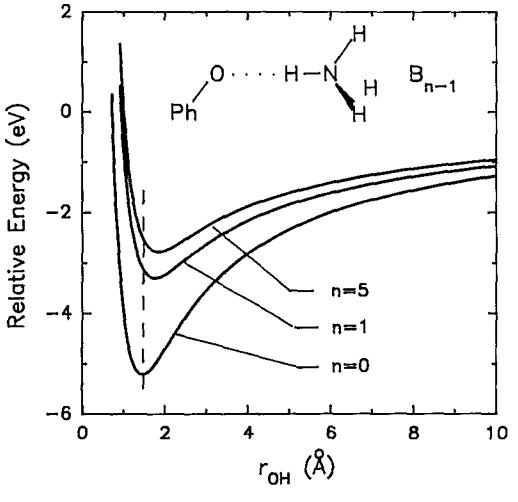

FIG. 13. Calculated Coulombic potentials for the $PhO^*\cdot H^+B_n$ ion-pair state as a function of the number of solvent molecules. Input parameters to Eq. (6) are $r_{Ph\text{-}O} = 2.5$ Å, $r_{H\text{-}N} = 1.04$ Å, $r_{N\text{-}H_3} = 0.52$ Å; $q_{ph} = -0.43$, $q_O = -0.57$; and for $n = 0$, $q_H = +1.0$; for $n = 1$, $q_H = 0.54$, $q_N = -1.01$, $q_{H_1} = 1.40$; for $n = 5$, $q_H = 0.48$, $q_N = -1.15$, $q_{H_3} = 1.50$. The repulsive parameters are $\beta = 100$ Å^{-1} and $\rho = 0.32$ Å. The dissociation limit is at zero relative energy. The dashed line corresponds to $r_e(n = 0)$.

The Coulombic attraction is a long-range interaction. Even at a separation of 10 Å, the ion pair is bound by $\geqslant$1 eV relative to the dissociative limit (Fig. 13). For the phenol monomer CT state ($n = 0$), the positive charge resides on the H atom (we assume $q_H = 1.0$) in close proximity to the negatively charged phenoxy. Hence, at the equilibrium position, the Coulombic well depth is relatively large ($V_e = -5.2$ eV) and the O–H bond length is short ($r_e = 1.4$–1.5 Å). A single NH_3 molecule delocalizes the positive charge, causing the ion-pair bond energy to decrease to $|V_e| = 3.1$ eV and the bond length to increase to 1.8 Å. Additional solvation further weakens and extends the O–H bond (e.g., $|V_e| = 2.7$ eV and $r_e = 1.9$ Å for $n = 5$).

The position of the ion-pair states in absolute energies varies with cluster size. The monomer CT states occur at very high energy as shown in Fig. 12(a). The dissociative limit to form $PhO^- + H^+$ relative to the ground electronic state of PhOH is obtained from the reported heat of deprotonation of 14.9 eV.[61] As a consistency check, a thermodynamic cycle can be written

$$\begin{aligned} &PhOH \rightarrow PhO + H, && D(PhO\text{–}H),\\ &H \rightarrow H^+ + e^-, && E_{I.P.}(H),\\ &PhO + e^- \rightarrow PhO^-, && -E_{E.A.}(PhO) \end{aligned}$$

that leads to the expression

$$\Delta H = D(\text{PhO–H}) + E_{\text{I.P.}}(\text{H}) - E_{\text{E.A.}}(\text{PhO}) \quad (7)$$
$$= 3.75 + 13.60 - 2.36 = 15.0 \text{ eV}$$

(where the values are from Refs. 54, 52, and 62, respectively). Deprotonation is clearly an unfavorable event in the isolated molecule. The dissociative energy to forming $PhO^{*-} + H^+$ is at 18.6 eV based on the PhO^{*-} excited state energy of 3.65 eV.[63,64] (We assume that the ground and excited ion-pair states have similar potential curves, even though the phenoxy charge distributions may be different.)

The $PhO^- H^+$ ion-pair states (and all states with large proton character) undergo a considerable energy shift when complexed to NH_3. The asymptotic limits of the potential curves that correlate to free H^+ are reduced in energy by an amount equal to the proton affinity of NH_3 {8.84 eV[51] [Fig. 12(b)]}. As the solvent size increases, the aggregate proton affinity increases (cf. Table I), which further stabilizes the ion-pair states. The bound state energies and dissociative limits are summarized in Table II as a function of solvent size n. The ion-pair potential curves for $n = 5$ are plotted in Fig. 13(c). The bonding energy $V^*_{e,n}$ of the excited state ion pair can be estimated from our experimental results. We interpret the observed ESPT threshold at $(NH_3)_5$ to mean that $\Delta H^*_4 > 0$ and $\Delta H^*_5 < 0$.[65] From Table II, we can place the following limits on the ion-pair bond energy: $|V^*_{e,4}| \leqslant 3.7$ eV and $|V^*_{e,5}| \geqslant 3.3$ eV. If we measure enthalpies from the zero-point energy rather than the minima energy of the locally excited and ion-pair potential curves, then the empirically derived values of $|V^*_{e,n}|$ decrease by about 0.3 eV. These values are in reasonable agreement with the calculated value of $|V_e| = 2.7$ eV for $n = 5$ (Fig. 13). Better agreement is expected once we include neglected effects listed above such as solvent stabilization of the anion.

VI. DYNAMICAL PROPERTIES OF THE SOLVENT

A. Direct measure of solvent reorganization in clusters

The kinetics for the ion-pair probe signal $H^+(NH_3)_n$ in Fig. 7 exhibit two time responses: a fast response of 60–70 ps that matches the decay constant for the reactant locally excited state and a slower response of about 0.3 ns. The latter response suggests some dynamical process that occurs after the initial proton transfer event. This observation is intriguing because it may represent a direct measure of solvent reorganization. Other explanations seem less plausible. The slow component is not due to a structural isomer, because this would also appear in the reactant decay curves. Evaporation can be ruled out for the following reasons: (1) evaporation in the neutral ion-pair state should show decay, not formation kinetics[66]; (2) dissociation from the cluster ion outer well does cause one or two solvent molecules to evaporate[15]; however, this process occurs after the λ_2 pulse and, therefore, the effect on intensity is independent of the pump–probe delay time.

A possible explanation for the dual time dependence is that the rapid 60–70 ps ESPT is followed by a slower process in which the solvent hydrogen-bond network reorganizes in response to the new electric-dipole forces imposed by the ion-pair structure. The initial ESPT involves an electron transfer and a geometry change along a single coordinate O–H. Therefore, it is expected to be a relatively fast process. The relaxation of the solvent involves many coordinates and should therefore be slower. Time-dependent ionization efficiencies are analogous to time-dependent Stokes shifts, the latter are used to measure structural reorganization in solution.[1] Both phenomena are due to changing Franck–Condon factors brought about by molecular motion.

The diagram in Fig. 14(a) illustrates how the potential energy along the O–H coordinate might change with time due to solvent reorganization. The equilibrium bond distance r_e for the neutral solvated ion-pair $PhO^{*-} H^+ B_n$ is about 1.8 Å[58] and is expected to increase slightly with increasing n (Fig. 13). The value of r_e in the cluster ion $PhO \cdot H^+ B_n$ should be greater because of the loss of Coulombic attraction (we assume 2 Å in paper II).[14] The neutral ion-pair $PhO^{*-} H^+ B_n$ structure that is formed on the 60 ps time scale retains much of the solvent bonding structure of the neutral excited state $PhOH^* \cdot B_n$ and is, therefore, a nonequilibrium structure with respect to solvation of the newly formed proton. The solvent network must reorganize to achieve a structure that best accommodates the proton (i.e., maximizes the proton affinity of the solvent shell). This reorganization represents solvation of the proton and causes

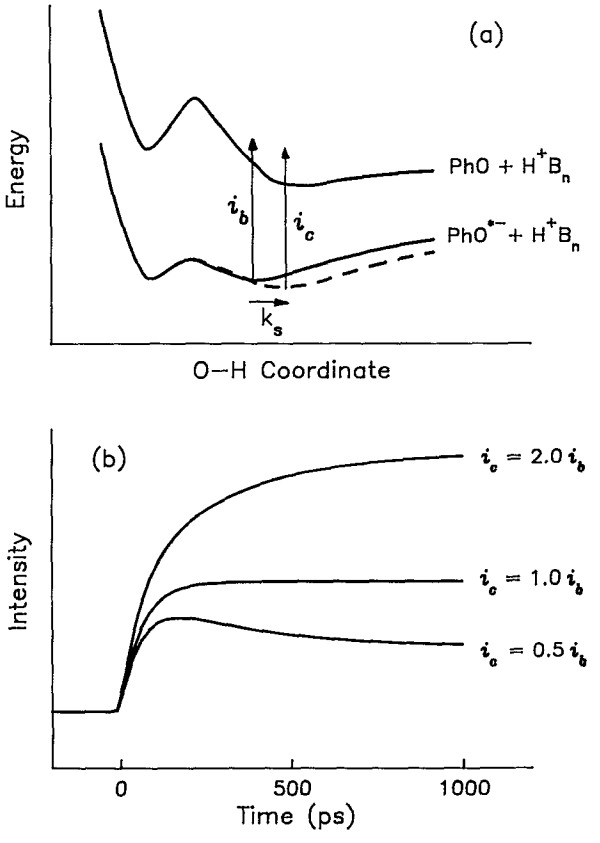

FIG. 14. (a) A schematic representation of the evolving solvent-relaxed ion-pair potential. (b) Calculated ion signal time dependence according to Eq. (8) for different relative values of the unrelaxed (i_b) and relaxed (i_c) ionization efficiencies. Other parameters used in the calculations were $f_a = 0, f_b = f_c = 1$, $1/k = 65$ ps, $1/k_s = 300$ ps.

delocalization of charge and lengthening of the O–H bond [Fig. 14(a)]. The relaxing ion pair moves toward a geometry similar to the cluster-ion equilibrium configuration. This improves the Franck–Condon factors for ionization and leads to increased ionization efficiency with time.

We modify Eq. (1) to include the production of a solvent-relaxed ion-pair structure with time constant $1/k_s$, ionization efficiency i_c and cluster-ion dissociative fraction f_c to give

$$P^+(t) = R^*(0)\{i_c f_c - [i_c f_c - A(t)]e^{-k_s t}\}, \quad (8)$$

where $A(t)$ is given by the term in braces in Eq. (2). If we assume that $f_a = 0$ then

$$A(t) = i_b f_b (1 - e^{-kt}). \quad (9)$$

This model treats the continuously evolving ion-pair structure as a two-state problem. The predicted response for different relative ionization efficiencies for relaxed vs unrelaxed solvent structures is shown in Fig. 14(b). The calculated curves through the data in Fig. 7 assume the values $1/k = 65$ ps and $1/k_s \simeq 0.3$ ns (see Fig. 7 caption). Similar parameters were fit to the $H^+(NH_3)_n$ traces recorded using $\lambda_2 = 355$ nm ionization (Fig. 8 only shows the early time data).

It is difficult to judge whether 0.3 ns is a reasonable time scale for solvent reorganization in $(NH_3)_n$ solvent clusters because we do not know the cluster temperatures. Most models of solvent reorientation about a dipole include more than one time constant, reflecting many types of molecular motion.[1] The fastest motions are due to bond rotations, whereas the slowest reorientations involve breaking and reforming of intermolecular solvent bonds. These would be particularly slow for hydrogen-bonded solvents. Extensive measurements of solvent relaxation for each of the reorientational degrees of freedom have been reported by many groups over a wide range of temperatures.[1,67–70] For the variety of solvents, molecular motions, and temperatures considered, relaxation times ranged from the experimentally detectable limit of about 100 fs[69] to greater than a nanosecond. The intermolecular motional time constant for ethanol at 253 K, e.g., was 112 ps (responding to a dipole excitation in a dye molecule). This is an activated process because of hydrogen-bond energy and, therefore, the rates vary significantly with temperature. We have not found any measurements of NH_3 solvent relaxation rates; however, it is certainly reasonable to expect the reorientation of hydrogen bonds at low temperatures ($\leqslant 100$ K) to be on the nanosecond time scale in accord with our experimental results.

B. Geminate ion-pair recombination

Because proton transfer is an equilibrium phenomena, one must consider the reverse rate constant k_-. The kinetic models of proton transfer in solution treat this process as a geminate ion-pair recombination and relate the rate to the competitive process of ion-pair separation[3]

$$PhOH^*\cdot B_n \underset{k_-}{\overset{k}{\rightleftarrows}} PhO^{*-}H^+B_n \rightarrow PhO^{*-}B_nH^+. \quad (10)$$

Picosecond measurements in solution have provided ample evidence for measurable values of k_- (by measurable, we mean equilibrium constants $K = k/k_-$ not far from unity).[21] The reactant time dependence (ignoring ion-pair separation) is given by

$$R^*(t) = \frac{k}{k+k_-}\left(e^{-(k+k_-)t} + \frac{k_-}{k}\right)R^*(0). \quad (11)$$

If the separation of the ion pair is slow relative to k_-, then the reactant signal decays to a plateau level of magnitude $R^*(0)k_-/(k+k_-)$.[71] This type of effect is observed in the decay traces of $[PhOH]^+\cdot(NH_3)_n$. For $n = 5$, a distinct plateau is observed that diminishes as n increases (Fig. 5).

The possibility that geminate ion-pair recombination is observable in clusters seems unlikely when considering the large stepwise solvation energies and low temperatures in clusters. The ratio of equilibrium constants for cluster sizes n and $n-1$ is given by

$$\ln\frac{K^*_n}{K^*_{n-1}} = (\Delta G^*_{n-1} - \Delta G^*_n)/kT \sim (\Delta H^*_{n-1} - \Delta H^*_n)/kT, \quad (12)$$

where we assume that $\Delta S_n \sim \Delta S_{n-1}$. The enthalpy change in going from $n = 4$ to $n = 5$ is 0.35 eV (Table II). The enthalpy change for $n = 5 \rightarrow 6$ is certainly > 0.10 eV. If we assume this lower limit and a cluster temperature of 100 K ($kT = 8.6\times10^{-3}$ eV/molecule), then we obtain a ratio of equilibrium constants of $K^*_5/K^*_5 > 10^4$. Although proton transfer studies in clusters enables *single molecule titration of acid-base reactions*, one cannot exercise fine control over the value of K. It will either be very large or very small. To make studies of geminate ion-pair recombination in clusters possible will require ESPT thresholds at larger solvent sizes and controllable cluster temperatures or energies.

The observed plateau in the decay curve for $n = 5$ can be explained by the model in Sec. III for incomplete cluster ion dissociation. The calculated curves in Fig. 5 assume for $n = 5$–7 values of $f_b = 0.92$, 0.96, and 0.97, respectively.

C. Solvent shell structure and evaporation

Bonding interactions involving solvent molecules play a vital role in chemistry. How solvent molecules aggregate about a reactive solute molecule has never been established experimentally. A variety of high-resolution spectroscopic methods have been able to determine the structure of a single solventlike molecule bound to a larger molecule (e.g., an aromatic);[72–74] however, as additional solvent molecules are added, the spectra often become too diffuse to be interpreted in terms of geometries. Instead, one can infer geometry and structural information from dynamical experiments.[49,50]

There are three primary outcomes following cluster ionization of $PhOH\cdot(NH_3)_n$:

$$[\mathrm{PhOH}]^+(\mathrm{NH_3})_n \rightarrow \begin{cases} [\mathrm{PhOH}]^+(\mathrm{NH_3})_n & \text{(no reaction)}, \quad (13a) \\ \mathrm{NH_4^+}(\mathrm{NH_3})_{n-1} + \mathrm{PhO} & \text{(DPT)}, \quad (13b) \\ [\mathrm{PhOH}]^+(\mathrm{NH_3})_{n-1} + \mathrm{NH_3} & \text{(evaporation)}, \quad (13c) \end{cases}$$

where DPT stands for dissociative proton transfer. The competition between reactions (13a)–(13c) depends primarily on two properties: (1) the binding energies and binding sites for each solvent molecule which differ with n and (2) on whether $[\mathrm{PhOH}]^+\cdot(\mathrm{NH_3})_n$ is formed in the first or second potential energy well (Fig. 2). Evaporation [reaction (13c)] from the inner potential well and from the reactant S_1 state (at least for $n<6$) is minor on the basis of the negligible residual of the $n=5$ curve on the $n=4$ curve (Fig. 5), and the weak phenol cation signal relative to the strong singly solvated phenol cation signal (Fig. 4). Other solvents also produce weak evaporative byproduct signals.

DPT [reaction (13b)] is the principal reaction from the outer potential well and occurs for $n>4$. The competition between DPT and evaporation [reaction (13c)] depends on whether the bond energies for the second-shell NH_3 molecules ($\leqslant 0.33$ eV) are greater than the $\mathrm{PhO}\cdots\mathrm{H}^+(\mathrm{NH_3})_n$ bond energy. One can argue that they are not. Because the proton affinities of PhO and NH_3 are reported to be similar,[75] one would expect that NH_3 in the second shell would dissociate (evaporate) more readily than PhO in the first shell. However, the $[\mathrm{PhOH}]^+\cdot(\mathrm{NH_3})_n$ decay curves in Fig. 5 would indicate otherwise. If reaction (13c) were prominent, a distinct residual baseline would be observed due to the accumulation of $[\mathrm{PhOH}]^+\cdot(\mathrm{NH_3})_n$ from larger clusters. Because such a residual signal is minimal (Fig. 5), it is concluded that DPT [reaction (13b)] dominates even when second-shell NH_3 molecules are present. An alternative explanation is that sufficient energy exists in the ion to evaporate all weakly bound NH_3 molecules *and* PhO.

Evaporation clearly occurs *following* DPT as witnessed by the abrupt disappearance of the $\mathrm{H}^+(\mathrm{NH_3})_n$ series for $n>5$. Analogous behavior occurs for TMA solvation, where the protonated $\mathrm{H}^+(\mathrm{TMA})_n$ series terminates abruptly for $n>2$. This is consistent with the solvent having a shell closing at $n=5$ for NH_3 and at $n=2$ for TMA. Ammoniated ammonium ion, which we write as $\mathrm{NH_4^+}(\mathrm{NH_3})_{n-1}$, has a stable closed-shell structure at $n=5$ corresponding to four NH_3 molecules that bond directly to the four protonic hydrogens of NH_4^+.[41] These first-shell solvent molecules have bond energies that range from 1.08 ($n=1$) to 0.54 eV ($n=4$). Additional NH_3 molecules add to the second shell and, therefore, have lower bond energies (Table I).[6] TMA does not have any proton donor sites and, therefore, has a protonated shell closing at $n=2$ with the structure $(\mathrm{CH_3})_3\mathrm{N}\cdot\mathrm{H}^+\cdot\mathrm{N}(\mathrm{CH_3})_3$. The termination of the observed $\mathrm{H}^+\mathrm{B}_n$ series at $n=5$ for NH_3 and $n=2$ for TMA argues that the hydrogen-bonding solvent structure about phenol is built around self-association of the solvent. Some stabilization of second-shell solvent molecules, however, may be gained by bonding to the phenoxy oxygen or to the aromatic ring.

VII. SUMMARY AND CONCLUSIONS

Proton transfer, which is the gas-phase terminology for acid-base reaction, is described by an electron transfer process, whereby a covalent bond is transformed to an ion-pair bond. The electron transfer is made possible by an environment (i.e., solvent) that can stabilize the ensuing proton. The movement of the electron is actually due to an electronic transition arising from a surface crossing. These properties characterize most proton transfer reactions. It is not obvious that these properties also describe solution-phase acid-base chemistry until one looks at the gas-phase counterpart and examines how the potential curves are changed by sequential addition of solvent molecules. The solvation properties in solution follow clearly from the cluster analogy.

We have presented a study of the prototype aromatic acid phenol seeded in clusters of solvent molecules. The rates and critical solvent sizes were measured for ESPT from phenol to a variety of pure and mixed solvent clusters. Our findings are summarized in the following:

(1) Proton transfer from S_1 phenol to $(\mathrm{NH_3})_n$ solvent clusters occurs abruptly at $n=5$ [$k=(60\pm 10\ \mathrm{ps})^{-1}$ for $n=5$–7]. Evidence of a reaction threshold in $\mathrm{N}(\mathrm{CH_3})_3$ ($n\simeq 3$) is also presented. Proton transfer was not observed in the less basic solvent clusters $(\mathrm{CH_3OH})_n$ and $(\mathrm{H_2O})_n$.

(2) In mixed solvent clusters $(\mathrm{NH_3})_n(\mathrm{CH_3OH})_m$, a PhOH* decay time of 750 ps was measured for $(m,n)=(5,1)$ vs 60 and 65 ps for (5,0) and (6,0). The reduction in reaction rate due to the presence of a single CH_3OH molecule is attributed to a disruption of an efficient $(\mathrm{NH_3})_n$ proton-accepting cluster core.

(3) Evidence is presented for the direct measure of solvent reorganization following ESPT. Solvent reorganization gives rise to a time-dependent Franck–Condon factor for ionization. A clearly observable long time-scale component (0.3 ns) was observed on the protonated solvent formation traces for $(\mathrm{NH_3})_n$ cluster solvation.

A model was developed to determine how the relevant potential energy curves for proton transfer are modified by sequential addition of solvent molecules. The following conclusions are obtained:

(4) The charge-transfer states of the isolated phenol molecule are responsible for gas-phase proton transfer and solution-phase acid-base chemistry. The high-energy dissociative limits of $\mathrm{PhO}^-\mathrm{H}^+$ (15.0 eV) and $\mathrm{PhO}^{*-}\mathrm{H}^+$ (18.6 eV), which yield a proton, are stabilized considerably by basic molecules such as NH_3 (e.g., $\Delta E=8.8$ eV for $n=1$). This results in a curve crossing with the locally excited states of S_1 and S_0.

(5) The ion-pair well depths, calculated using a Coulomb potential and reported theoretical charge distributions, decrease from $V_e=-5.2$ eV ($n=0$) to $V_e=-2.7$

eV, reflecting the delocalization of the proton charge through the $(NH_3)_n$ hydrogen-bonding network.

(6) For the ion-pair states of phenol, about 50% of the bulk proton stabilization energy is provided by the first NH_3 molecule and about 90% by the first shell closing at $n = 4$ or $n = 5$. This analysis is based on aggregate proton affinity only and ignores other contributions to bulk dielectric polarization effects.

These analyses have provided a consistent framework for investigating the solvation of a chemical reaction on a molecular level. The solvent properties are not governed by energetics alone, but also by specific structural stabilities. We have gained important insight into solvent structure and the relative importance of first- and second-shell solvent molecules.

The combination of time-resolved spectroscopy and mass-selective detection holds great promise for studying complex reaction mechanisms in size-specific neutral clusters. Although the techniques are now well established for studying stepwise solvation, the work reported here shows that picosecond mass-selective measurements of rapid *intermolecular* photochemistry in clusters offers a new domain for studying the molecular basis of solvation on reactive systems.

ACKNOWLEDGMENT

This work was supported by the Aerospace Sponsored Research program.

[1] M. Maroncelli, J. MacInnis, and G. R. Fleming, Science **243**, 1674 (1989); J. D. Simon, Acc. Chem. Res. **21**, 128 (1988).
[2] I. Rips, J. Klafter, and J. Jortner, J. Chem. Phys. **88**, 3246 (1988); M. Sparpaglione and S. Mukamel, *ibid.* **88**, 3263 (1988).
[3] E. Pines, D. Huppert, and N. Agmon, J. Chem. Phys. **88**, 5620 (1988); N. Agmon, D. Huppert, and E. Pines, *ibid.* **88**, 5631 (1988).
[4] J. N. Onuchic and P. G. Wolynes, J. Phys. Chem. **92**, 6495 (1988).
[5] B. M. Pettitt and P. J. Rossky, J. Chem. Phys. **84**, 5836 (1986).
[6] P. Kebarle, Ann. Rev. Phys. Chem. **28**, 445 (1977); E. P. Grimsrud and P. Kebarle, J. Am. Chem. Soc. **95**, 7939 (1973).
[7] J. J. Breen, W.-B. Tzeng, K. Kilgore, R. G. Keesee, and A. W. Castleman, Jr., J. Chem. Phys. **90**, 19 (1989); O. Echt, P. D. Dao, S. Morgan, and A. W. Castleman, Jr., *ibid.* **82**, 4076 (1985); S. Morgan and A. W. Castleman, Jr., J. Am. Chem. Soc. **109**, 2867 (1987).
[8] O. Cheshnovsky and S. Leutwyler, J. Chem. Phys. **88**, 4127 (1988); T. Droz, R. Knochenmuss, and S. Leutwyler, *ibid.* **93**, 4520 (1990); R. Knochenmuss, O. Cheshnovsky, and S. Leutwyler, Chem. Phys. Lett. **144**, 317 (1988).
[9] P. M. Felker and A. H. Zewail, Chem. Phys. Lett. **94**, 448 (1983); **94**, 454 (1983); L. W. Peng, M. Dantus, A. H. Zewail, K. Kemnitz, J. M. Hicks, and K. B. Eisenthal, J. Phys. Chem. **91**, 6162 (1987); J. A. Warren and E. R. Bernstein, J. Seeman, J. Chem. Phys. **88**, 871 (1987).
[10] C. Jouvet, C. Lardeux-Dedonder, M. Richard-Viard, D. Solgadi, and A. Tramer, J. Phys. Chem. **94**, 5041 (1990); D. Solgadi, C. Jouvet, and A. Tramer, *ibid.* **92**, 3313 (1988).
[11] J. A. Syage, J. Chem. Phys. **92**, 1804 (1990); J. Phys. Chem. **93**, 107 (1989).
[12] J. A. Syage and J. Steadman, Chem. Phys. Lett. **166**, 159 (1990).
[13] J. Steadman and J. A. Syage, J. Chem. Phys. **92**, 4630 (1990).
[14] J. Steadman and J. A. Syage, J. Am. Chem. Soc. **113** (1991).
[15] J. Steadman, E. W. Fournier, and J. A. Syage, Appl. Opt. **29**, 4962 (1990); J. A. Syage, SPIE Proc. **1209**, 64 (1990).
[16] D. Ray, N. E. Levinger, J. M. Papanikolas, and W. C. Lineberger, J. Chem. Phys. **91**, 6533 (1989).
[17] J. J. Breen, L. W. Peng, D. M. Willberg, A. Heikal, P. Cong, and A. H. Zewail, J. Chem. Phys. **92**, 805 (1990).
[18] *Proton Transfer Reactions*, edited by E. Caldin and V. Gold (Wiley, New York, 1975).
[19] E. M. Kosower and D. Huppert, Ann. Rev. Phys. Chem. **37**, 127 (1986); P. M. Rentzepis and P. F. Barbara, Adv. Chem. Phys. **47**, 627 (1981); E. S. Lewis, in *Proton Energy Transfers*, edited by E. Caldin and V. Gold (Wiley, New York, 1975), p. 317.
[20] K. K. Smith, K. J. Kaufmann, D. Huppert, and M. Gutman, Chem. Phys. Lett. **64**, 522 (1979); H. Shizuka, K. Tsutsumi, H. Takeuchi, and I. Tanaka, *ibid.* **62**, 408 (1979).
[21] D. H. Huppert, A. Jayaraman, R. G. Maines, Sr., D. W. Steyert, and P. M. Rentzepis, J. Chem. Phys. **81**, 5596 (1984); D. Huppert, E. Kolodney, M. Gutman, and E. Nachliel, J. Am. Chem. Soc. **104**, 6949 (1982).
[22] S. P. Webb, L. A. Philips, S. W. Yeh, L. M. Tolbert, and J. H. Clark, J. Phys. Chem. **90**, 5154 (1986).
[23] C. R. Moylan and J. I. Brauman, Ann. Rev. Phys. Chem. **34**, 187 (1983).
[24] N. G. Adams, D. Smith, and J. F. Paulson, J. Chem. Phys. **72**, 288 (1980).
[25] W. R. Lambert, P. M. Felker, and A. H. Zewail, J. Chem. Phys. **75**, 5958 (1981); J. A. Syage, W. R. Lambert, P. M. Felker, A. H. Zewail, and R. M. Hochstrasser, Chem. Phys. Lett. **88**, 266 (1982); A. H. Zewail, Faraday Discuss. Chem. Soc. **75**, 315 (1983).
[26] J. L. Knee, L. R. Khundkar, and A. H. Zewail, J. Chem. Phys. **82**, 4715 (1985); N. F. Scherer, J. L. Knee, D. D. Smith, and A. H. Zewail, J. Phys. Chem. **89**, 5141 (1985); L. R. Khundkar, J. L. Knee, and A. H. Zewail, J. Chem. Phys. **87**, 77 (1987).
[27] M. Dantus, M. J. Rosker, and A. H. Zewail, J. Chem. Phys. **87**, 2395 (1987); T. S. Rose, M. J. Rosker, and A. H. Zewail, *ibid.* **88**, 6672 (1988); A. H. Zewail, Science **242**, 1645 (1989).
[28] J. L. Knee, L. R. Khundkar, and A. H. Zewail, J. Chem. Phys. **87**, 115 (1987); D. H. Semmes, J. S. Baskin, and A. H. Zewail, J. Am. Chem. Soc. **109**, 4104 (1987).
[29] M. P. Cassasa, J. C. Stephenson, and D. S. King, J. Chem. Phys. **89**, 1966 (1988). A. J. Kazishka, M. I. Shchuka, S. A. Wittmeyer, and M. R. Topp, J. Phys. Chem. **95**, 3663 (1991).
[30] D. H. Semmes, J. S. Baskin, and A. H. Zewail, J. Chem. Phys. **92**, 3359 (1990); M. R. Nimlos, M. A. Young, E. R. Bernstein, and D. F. Kelley, *ibid.* **91**, 5268 (1989); K. Rademann, U. Even, S. Rozen, and J. Jortner, Chem. Phys. Lett. **125**, 5 (1986).
[31] *Dynamics of Polyatomic van der Waals Complexes*, edited by N. Halberstadt and K. C. Janda (NATO ASI, Washington, D.C., 1990), Vol. 227.
[32] G. A. Brucker and D. F. Kelley, J. Chem. Phys. **90**, 5243 (1989); G. A. Brucker and D. F. Kelley, Chem. Phys. Lett. **136**, 213 (1989).
[33] W. C. Wiley and I. H. McLaren, Rev. Sci. Instrum. **26**, 1150 (1955).
[34] If reactant and product ionization involve the same number of photons, then the ratio of i_a and i_b is equivalent to the ratio of cross sections.
[35] N. Mikami, A. Okabe, and I. Suzuki, J. Phys. Chem. **92**, 1858 (1988).
[36] N. Mikami, I. Suzuki, and A. Okabe, J. Phys. Chem. **91**, 5242 (1987).
[37] R. J. Lipert and S. D. Colson, J. Phys. Chem. **94**, 2358 (1990); J. Chem. Phys. **89**, 4579 (1988); R. J. Lipert, G. Bermudez, and S. D. Colson, J. Phys. Chem. **92**, 3801 (1988).
[38] N. Gonohe, H. Abe, N. Mikami, and M. Ito, J. Phys. Chem. **89**, 3642 (1985); A. Oikawa, H. Abe, N. Mikami, and M. Ito, *ibid.* **87**, 5083 (1983).
[39] P. J. Robinson and K. A. Holbrook, *Unimolecular Reactions* (Wiley, New York, 1972).
[40] C. A. Deakyne, J. Phys. Chem. **90**, 6625 (1986).
[41] J. M. Price, M. W. Crofton, and Y. T. Lee, J. Chem. Phys. **91**, 2749 (1989); J. Phys. Chem. **95**, 2182 (1991).
[42] J. Lee, R. D. Griffin, and G. W. Robinson, J. Chem. Phys. **82**, 4920 (1985); J. Lee, G. W. Robinson, S. P. Webb, L. A. Philips, and J. H. Clark, J. Am. Chem. Soc. **108**, 6538 (1986); J. Lee and G. W. Robinson, J. Chem. Phys. **81**, 1203 (1984).
[43] D. Huppert, E. Kolodney, M. Gutman, and E. Nachliel, J. Am. Chem. Soc. **104**, 6949 (1982).
[44] The $S_1 \leftarrow S_0$ transition of phenol is red shifted by the addition of one CH_3OH molecule and blue shifted by the addition of a second molecule. These observations indicate that CH_3OH bonds first to the hydroxy and then to the oxygen of phenol (Refs. 35–37). No blue shift is observed for any successive addition of NH_3 to phenol, indicating that it does not bond to the oxygen. This is consistent with NH_3 being a good proton acceptor, but a poor proton donor (Ref. 45).
[45] D. D. Nelson, Jr., G. T. Fraser, and W. Klemperer, Science **238**, 1670 (1987).
[46] J. D. Payzant, A. J. Cunningham, and P. Kebarle, Can. J. Chem. **51**, 3242 (1973); Y. K. Lau, S. Ikuta, and P. Kebarle, J. Am. Chem. Soc. **104**, 1462 (1982).
[47] G. C. Pimentel and A. L. McClellan, *The Hydrogen Bond* (Freeman, San

Francisco, 1960).
[48] C. E. Dykstra, J. Phys. Chem. **94**, 6948 (1990).
[49] S. Wei, Z. Shi, and A. W. Castleman, Jr. J. Chem. Phys. **94**, 3268 (1991).
[50] J. Steadman and J. A. Syage. J. Phys. Chem. **95** (1991).
[51] S. G. Lias, J. F. Liebman, and R. D. Levin, J. Phys. Chem. Ref. Data **13**, 695 (1984).
[52] S. G. Lias, J. E. Bartmess, J. F. Liebman, J. L. Holmes, R. D. Levin, and W. G. Mallard, J. Phys. Chem. Ref. Data **17**, 1 (1988).
[53] Mikami, *et al.* (Ref. 36) report that only protonated H^+(TMA), and not TMA^+, is observed in the resonance ionization measurements of PhOH·TMA; however, their published mass spectrum does not appear to have adequate resolution to distinguish between these two product ions.
[54] D. F. McMillen and D. M. Golden, Ann. Rev. Phys. Chem. **33**, 493 (1982) and references therein.
[55] Calculated from the expressions $A = (2E/k)^{1/2}$ and $\nu = (k/\mu)^{1/2}/2\pi$, where A is the amplitude, k is the force constant, μ is the reduced mass, and we set $E = 3h\nu/2$.
[56] T. P. Martin, J. Chem. Phys. **72**, 3506 (1980).
[57] A. Pross, L. Radom, and R. W. Taft, J. Am. Chem. Soc. **45**, 818 (1980).
[58] A. Matsuyama and A. Imamura, Bull. Chem. Soc. Jpn. **45**, 2196 (1972).
[59] The ion-pair potential was plotted using the repulsive parameters $\beta = 100$ Å^{-1} and $\rho = 0.32$ Å. These values are consistent with computed ion-pair potentials of alkali halides in water (Ref. 5).
[60] E. M. Arnett, in *Proton-Transfer Reactions*, edited by E. Caldin and V. Gold (Wiley, New York, 1975), p. 79.
[61] M. Fujio, R. T. McIver, Jr., and R. W. Taft, J. Am. Chem. Soc. **103**, 4017 (1981).
[62] C. R. Moylan and J. I. Brauman, Ann. Rev. Phys. Chem. **34**, 187 (1983); P. B. Comita and J. I. Brauman, Science **227**, 863 (1985).
[63] J. H. Richardson, L. M. Stephenson, and J. I. Brauman, J. Am. Chem. Soc. **97**, 2967 (1975).
[64] An alternative PhO^{*-} excited state energy of 4.32 eV was also considered by Solgadi, *et al.* (Ref. 10) from an early work [K. Nishimoto and L. S. Forster, J. Phys. Chem. **72**, 914 (1968)].
[65] We assume $T\Delta S \sim 0$ because ΔS is small and the clusters are cold; hence, $\Delta H^* \sim \Delta G^*$.
[66] Evaporation from larger clusters can contribute to the signal for a smaller cluster; however, we employed a decreasing cluster size distribution to minimize this problem.
[67] S-G. Su and J. D. Simon, J. Chem. Phys. **89**, 908 (1988).
[68] M. Kozik, N. Sutin, and J. R. Winkler, Coord. Chem. Rev. **97**, 23 (1990).
[69] W. Jarzeba, G. C. Walker, A. E. Johnson, M. A. Kahlow, and P. F. Barbara, J. Phys. Chem. **92**, 7039 (1988).
[70] M. Maroncelli and G. R. Fleming, J. Chem. Phys. **86**, 6221 (1987).
[71] If the instrument temporal response is not much shorter than $1/k$, then the peak intensity will be rounded off and the long-time plateau signal will appear accentuated.
[72] L. A. Peteanu and D. H. Levy, J. Phys. Chem. **92**, 6554 (1988); B. D. Howells, M. T. Martinez, T. F. Palmer, J. P. Simons, and A. Walters, J. Chem. Soc. Faraday Trans. **86**, 1949 (1990).
[73] L. L. Connell, T. C. Corcoran, P. W. Joireman, and P. M. Felker, J. Phys. Chem. **94**, 1229 (1990).
[74] B. B. Champagne, J. F. Pfanstiel, D. F. Plusquellic, D. W. Pratt, W. M. van Herpen, and W. L. Meerts, J. Phys. Chem. **94**, 6 (1990).
[75] The proton affinity of NH_3 and PhO are both reported to be 8.8 eV (Ref. 51); however, PhO must have a lower proton affinity in order to account for the prominence of reaction (13b).
[76] S. T. Ceyer, P. W. Tiedemann, B. H. Mahan, and Y. T. Lee, J. Chem. Phys. **70**, 14 (1979); J. C. Greer, R. Ahlrichs, and V. Hertel, Chem. Phys. **133**, 191 (1989).
[77] M. F. Vernon, D. J. Krajnovich, H. S. Kwok, J. M. Lisy, Y. R. Shen, and Y. T. Lee, J. Chem. Phys. **77**, 47 (1982).